Solution Structure and Orientation of the Transmembrane Anchor Domain of the HIV-1-Encoded Virus Protein U by High-Resolution and Solid-State NMR Spectroscopy†

Victor Wray,*,‡,§ Rudolf Kinder,§,|| Torsten Federau,‡,§ Peter Henklein,⊥ Burkhard Bechinger,*,|| and Ulrich Schubert#,@

Department of Molecular Structure Research, Gesellschaft für Biotechnologische Forschung, Braunschweig, Germany, Max-Planck-Institut für Biochemie, Bereich Strukturforschung, Martinsried, Germany, Institute of Biochemistry, Humboldt University, Berlin, Germany, Laboratory of Viral Diseases, National Institute of Allergy and Infectious Diseases, National Institutes of Health, Bethesda, Maryland 20892, and Heinrich-Pette-Institute of Experimental Virology, University of Hamburg, Hamburg, Germany

Received November 19, 1998; Revised Manuscript Received February 9, 1999

ABSTRACT: The structure of the membrane anchor domain (Vpu_{MA}) of the HIV-1-specific accessory protein Vpu has been investigated in solution and in lipid bilayers by homonuclear two-dimensional and solid-state nuclear magnetic resonance spectroscopy, respectively. Simulated annealing calculations, using the nuclear Overhauser enhancement data for the soluble synthetic peptide Vpu^{1-39} (positions Met-1−Asp-39) in an aqueous 2,2,2-trifluoroethanol (TFE) solution, afford a compact well-defined U-shaped structure comprised of an initial turn (residues 1−6) followed by a linker (7−9) and a short helix on the N-terminal side (10−16) and a further longer helix on the C-terminal side (22−36). The side chains of the two aromatic residues (Trp-22 and Tyr-29) in the longer helix are directed toward the center of the molecule around which the hydrophobic core of the folded Vpu_{MA} is positioned. As the observed solution structure is inconsistent with the formation of ion-conductive membrane pores defined previously for Vpu_{MA} in planar lipid bilayers, the isolated Vpu_{MA} domain as peptide Vpu^{1-27} was investigated in oriented phospholipid bilayers by proton-decoupled ^{15}N cross polarization solid-state NMR spectroscopy. The line widths and chemical shift data of three selectively ^{15}N-labeled peptides are consistent with a transmembrane alignment of a helical polypeptide. Chemical shift tensor calculations imply that the data sets are compatible with a model in which the nascent helices of the folded solution structure reassemble to form a more regular linear α-helix that lies parallel to the bilayer normal with a tilt angle of ≤30°. The arrangement of the membrane-associated structures described previously for the cytoplasmic domain and for the anchor domain of Vpu identified in this work is discussed.

The human immunodeficiency virus type 1 (HIV-1)[1] is a member of the primate lentivirus subfamily of retroviridae that also include HIV-2 and SIV. Besides typical structural retrovirus and enzymatically active proteins, HIV-1 also encodes several small regulatory proteins. One of these, the viral protein U (Vpu), has an accessory function for the viral life cycle and seems to be specific for HIV-1 (*1*, *2*) since no structural and functional homology has been identified for other primate lentiviruses except for the HIV-1-related chimpanzee isolate SIV_{CPZ} (*3*).

A substantial amount of biochemical data exists that characterize Vpu as a type I oriented integral oligomeric membrane phosphoprotein composed of an amphipathic sequence of 81 amino acids comprising a hydrophobic N-terminal membrane anchor (Vpu_{MA}) proximal to a polar C-terminal cytoplasmic domain (Vpu_{CYTO}) (*4*−*6*). The latter contains a highly conserved region, from Glu-47 to Gly-58 (*3*, *7*), which contains two seryl residues that are phosphorylated by casein kinase 2 (CK-2) in HIV-1-infected cells (*8*, *9*). Proteinase K digestion of membrane-integrated Vpu indicated that Vpu_{MA} is located at the N-terminus and contains less than 30 residues (*6*). Reconstitution of synthetic Vpu_{MA} in planar lipid bilayers identified a cation-selective ion channel activity (*10*) which was also demonstrated for

† This work was supported by Grant SCHU1125 and by a "Heisenberg" fellowship from the Deutsche Forschungsgesellschaft to U.S.

* Corresponding authors. V.W.: Abteilung für Strukturforschung, GBF-Gesellschaft für Biotechnologische Forschung mbH, Mascheroder Weg 1, D-38124 Braunschweig, Germany; fax, +531 6181 355; e-mail, vwr@gbf.de. B.B.: Max-Planck-Institut für Biochemie, Bereich Strukturforschung, Am Klopferspitz 18a, D-82152 Martinsried, Germany; fax, +89 8578 2876; e-mail, bechinge@alf.biochem.mpg.de.

‡ Gesellschaft für Biotechnologische Forschung.

§ These authors contributed equally to this work.

|| Max-Planck-Institut für Biochemie.

⊥ Humboldt University.

National Institutes of Health.

@ University of Hamburg.

[1] Abbreviations: CD, circular dichroism; COSY, correlation spectroscopy; ER, endoplasmic reticulum; HIV, human immunodeficiency virus; MD, molecular dynamics; $M2_{TM}$, transmembrane anchor domain of the influenza A virus M2 protein; NMR, nuclear magnetic resonance; NOE, nuclear Overhauser enhancement; NOESY, nuclear Overhauser and exchange spectroscopy; rms, root-mean-square; TFE, 2,2,2-trifluoroethanol; TOCSY, total correlation spectroscopy; Vpu_{MA}, membrane anchor domain of Vpu; Vpu_{CYTO}, cytoplasmic domain of Vpu.

10.1021/bi982755c CCC: $18.00
Published on Web 03/31/1999

full-length Vpu in bilayers (*11*) and in amphibian oocytes (*10*).

Functionally, Vpu is involved in two distinct processes in the viral life cycle. First, it regulates virus release from a post-ER compartment (*2*, *4*, *5*, *12*, *13*), and second, it contributes selectively to the downregulation of host cell receptor proteins such as CD4, the major cellular receptor for HIV-1 (*14*), and major histocompatibility complex (MHC) class I molecules (*15*). Recent studies demonstrated that Vpu-induced degradation of CD4 requires physical interaction between the ER membrane-associated CD4 and Vpu (*16*), the CK-2-mediated phosphorylation of two conserved serine residues in Vpu_{CYTO} (*8*, *17*−*19*), the formation of multiprotein complexes containing CD4, Vpu, hβTrCp, and Skp1 (*20*), and the function of the ubiquitin−proteasome pathway (*21*, *22*).

The structural and functional architecture of Vpu are related as the CD4 degradation function involves activities residing in Vpu_{CYTO}, while the virion release function is mediated by the cation-selective ion channel activity residing in Vpu_{MA} (*10*, *11*, *13*; reviewed in ref *23*). Although considerable effort has been spent elucidating the molecular mechanism of Vpu in the ER, only scant attention has been paid to understanding Vpu's second function, the ion channel-mediated augmentation of virus particle release, an activity strictly dependent on the integrity of the primary sequence of Vpu_{MA} (*13*).

Similarly, while considerable work by CD and NMR spectroscopy has been focused solely on the structural analysis of Vpu_{CYTO}, no experimental work has been focused on Vpu_{MA}, apart from structural predictions (*4*, *9*, *10*, *13*, *24*, *25*). For Vpu_{CYTO}, evidence has been presented, using two-dimensional homonuclear NMR spectroscopy, of a well-defined helix−interconnection−helix−turn secondary structure for this domain in aqueous organic solutions (*26*−*28*) and a tertiary folded structure with essentially the same secondary structural elements in an organic-free high-salt aqueous solution (*29*). To date, however, no direct experimental evidence has been reported for the structure of Vpu_{MA}, although there is biochemical data which suggest that the N-terminal hydrophobic domain exists as a transmembrane anchor (*6*) that has the ability to function as an ion channel by itself (*10*) or in the context of full-length Vpu (*11*). How this ion channel activity might mediate the virion release function of Vpu is still unknown. Theoretical models of the Vpu channel have been generated using restrained MD which concludes that the most likely mechanism for its formation is through Vpu_{MA} adopting an α-helical structure and formation in the bilayer of an oligomer of five approximately parallel helices surrounding a central aqueous pore (*24*). More recent calculations indicated that Vpu_{MA} may form a pentameric helix bundle with a cone-like C-terminal region that in some motives resembles the structure of a typical potassium channel (25). Clearly, these investigations place considerable onus on the establishment of experimental evidence for the structure of Vpu_{MA}.

Whereas solution NMR spectroscopy provides information about the propensity of linear peptides to maintain secondary structure, complimentary solid-state NMR techniques can provide details about the structure and dynamics of these peptides when associated with lipid bilayers that simulate the natural membrane environment (reviewed in ref *30*). In addition, ^{15}N solid-state NMR spectroscopy of isotopically labeled peptides incorporated into either mechanically or magnetically aligned membranes provides a means of determining the orientation of the NH vectors and, therefore, α-helical domains with respect to the bilayer normal. Thus, once the positions of helical secondary structure of the membrane-bound peptide have been established, a single spectral parameter, namely, the solid-state ^{15}N chemical shift, is sufficient to define the approximate helix orientation relative to the plane of the membrane bilayer (*31*). We, therefore, resolved to combine these techniques during our structural analysis of the Vpu_{MA} domain.

In previous electrophysiological studies, we have used a synthetic peptide, Vpu^{1-27}, comprising the entire Vpu_{MA} domain to characterize the cation-selective channel activity of Vpu_{MA} in planar lipid bilayers (*10*). However, the limited solubility of this hydrophobic peptide in aqueous solutions prevented investigations by high-resolution NMR. The solubility of peptides containing the Vpu_{MA} sequence was significantly improved upon incorporation of the first 12 hydrophilic amino acids of Vpu_{CYTO} that comprise the N-terminal region of the first cytoplasmic helix (*27*, *28*). In the work presented here, we demonstrate that the resulting peptide, Vpu^{1-39}, has a well-defined tertiary structure comprising a U-formed α-helical conformation under optimal solution conditions that were established by CD spectroscopy. Subsequent solid-state NMR data for the peptide Vpu^{1-27} provide compelling evidence that in the membrane-like environment of oriented lipid bilayers Vpu_{MA} undergoes a substantial rearrangement of the folded structure found in solution and adopts a stable linear helical structure in a transmembrane orientation.

EXPERIMENTAL PROCEDURES

Peptide Synthesis. The peptides were synthesized as the C-terminal amides and purified by reverse-phase HLPC as described previously by us for other fragments of Vpu (*26*). Specific singly ^{15}N-labeled peptides with labels in position 10, 14, or 18 were synthesized by the use of the appropriate labeled [^{15}N]Fmoc amino acid derivatives obtained from Cambridge Isotope Laboratories (Andover, MA). Because of the limited solubility caused by the presence of a majority of hydrophobic residues in the Vpu_{MA} sequence, all peptides were dissolved in water/TFE mixtures for purification purposes. The purity of each peptide was checked by N-terminal sequencing, and the correct molecular weights were established by negative ion electrospray mass spectrometry. The sequences of peptides Vpu^{1-27} and Vpu^{1-39} (see Figure 2 for the sequences) correspond to that of the Vpu protein encoded by the HIV-1 isolate HXB10 (*32*). The peptide Vpu^{1-27} was previously used to study the ion channel characteristics of Vpu_{MA} in planar lipid bilayers (*10*). Two further peptide variants of Vpu^{1-39} were synthesized: Vpu_a^{1-39}, with the first six N-terminal residues ^{1}MQPIIV^6 corresponding to the Vpu protein of the HIV-1 ioslate NL4-3 (*32*, *33*), and Vpu_b^{1-39}, with the first six N-terminal residues ^{1}MQPIQI^6 corresponding to the Vpu protein of the HIV-1 ioslate LAI (*32*). Because of the better solubility in aqueous TFE, the peptide Vpu_a^{1-39} was used for the CD investigation while Vpu_b^{1-39} was used as a control peptide for solution NMR in addition to the peptide Vpu^{1-39}.

CD Spectroscopy. Spectra of Vpu_a^{1-39} (0.1 mg/mL) dissolved in aqueous TFE were measured at ambient temperature in 1 mm curvettes on a Jasco J-600 CD spectrometer. TFE mixtures in the range of 10−100% TFE were measured, although in the lower TFE range (10−20%) solution turbidity was observed. As the CD curves are concentration-dependent, the curves in this range cannot be directly compared with those at the higher TFE concentrations but are included in Figure 1 for completeness.

NMR Spectroscopy. For the solution experiments, samples of peptide (Vpu^{1-39}, 4 mg) were dissolved in distilled water containing 50% TFE-d_2 by volume to give a final volume of 0.6 mL at pH 3.7 [TFE-d_2 was produced by fractional distillation of a 1:1 mixture of H_2O and TFE-d_3 (Merck, Darmstadt, Germany)]. Spectra were recorded at 299 K on a Bruker AM 600 instrument without spinning using a dedicated 5 mm proton probehead and temperature unit (Haake, Karlsruhe, Germany). The ^{1}H spectra were referenced to sodium 4,4-dimethyl-4-silapentane-1-sulfonate and indirectly to the residual signal of TFE at 3.95 ppm. Two-dimensional phase-sensitive ^{1}H COSY, TOCSY (mixing times of 70 ms), and NOESY (mixing times of 150 ms) spectra were recorded and processed as described previously (*33*).

For solid-state NMR measurements, 15 mg of each of the three differentially ^{15}N labeled Vpu^{1-27} peptides were dissolved in 2 mL of hexafluoro-2-propanol (HFIP) and the pH was adjusted to pH 5. After addition of 300 mg of 1-palmitoyl-2-oleoyl-*sn*-glycero-3-phosphocholine (POPC), the solution was spread onto 25 cover glasses (22 mm × 11 mm × 0.07 mm). To ensure the removal of all organic solvent, the samples were first dried in air and thereafter exposed to high vacuum overnight (<0.1 mbar). The samples were equilibrated in 93% relative humidity before the cover glasses were stacked on top of each other.

For solid-state NMR spectroscopy, the samples were tightly sealed, inserted into a homemade flat-coil probehead (*34*), and introduced into the magnet with the bilayer normal parallel to the magnetic field. In this arrangement, the main axis of rotational diffusion within the lipid bilayer coincides with the magnetic field direction and, therefore, oriented solid-state NMR spectra are observed. Proton-decoupled ^{15}N solid-state NMR spectra were recorded using a Bruker AMX 400 wide bore NMR spectrometer equipped with a MSL high-power cabinet. For signal enhancement, a cross polarization pulse sequence (*35*) with the following parameters was used: recycle delay of 3 s, spin-lock time of 0.8 ms, 90° ^{1}H pulse lasting 4 μs, acquisition time of 3.2 ms, 256 data points, ^{1}H decoupling field ca. 1 mT, and 10 000 transients. During the measurements, the sample was cooled with a stream of air. An exponential apodization function of 200 Hz was applied before Fourier transformation, and spectra were calibrated with respect to [^{15}N]ammonium sulfate (27 ppm), although shifts are reported with respect to liquid NH_3.

NMR Solution Spectral Assignments. A standard procedure (*36*) was used to establish the unambiguous amino acid spin systems, sequential assignments, and final medium- and long-range NOEs. Even though there are many hydrophobic residues in Vpu_{MA}, the signal assignments presented no problems as the amide signals are evenly distributed over the region of 7.40−9.00 ppm which is considerably better than that observed for a previously analyzed peptide, Vpu^{32-81} (*27*) comprising the Vpu_{CYTO} domain, and can be taken as a first indication of a well-defined structure in Vpu_{MA}. The complete signal assignments and ^{1}H chemical shifts are available.

Structure Calculations. The volumes of the integrated cross-peaks from the NOESY spectra were determined using the AURELIA program (*37*), and distances were calibrated against the side chain Gln and terminal amide protons (0.19 nm). Structures were then generated using a standard restrained molecular dynamics protocol as described previously (*38*) using the program X-PLOR version 3.1 (*39*) on a DEC VAX 3000 Alpha workstation (Digital Equipment Corp., Maynard, MA). The resulting structures were displayed on a Hewlett-Packard Apollo graphic workstation (Hewlett-Packard Co., Palo Alto, CA) using the program BRAGI (version 5.0) (*40*). Structure fitting criteria were objectively derived using a consecutive segment method described by us previously (*41*) that employs modified programs from X-PLOR.

RESULTS

The original aim of our study was to analyze the structure of the Vpu_{MA} domain whose sequence position in Vpu was previously predicted on the basis of hydrophobic plot analysis (*2*, *5*, *9*) and protease K digestion studies (*6*). It was assumed that Vpu_{MA} comprises the first 27 N-terminal amino acids of Vpu by which the peptide is cotranslationally integrated into the ER membrane (*4*). We were particularly interested in the structure of Vpu_{MA} since we and others (*10*, *11*) have previously defined a cation-selective ion channel activity that regulates the virus release function of Vpu (*13*).

Preliminary experiments quickly established that peptides comprising solely the hydrophobic Vpu_{MA} region are almost completely insoluble in aqueous solution even in the presence of organic solvents. To circumvent this problem, we were able to increase the solubility of these peptides by incorporating the first 12 polar residues of Vpu_{CYTO}. The resulting peptide Vpu^{1-39}, which was even soluble in a pure aqueous solution containing small amounts of the membrane mimetic TFE, could be conveniently synthesized and was obtained in a highly purified state as described in Experimental Procedures. The sequence of Vpu^{1-39} was derived from the HIV-1 isolate HXB10 (*32*) that encodes a biologically active Vpu protein (*12*) and corresponds to the synthetic Vpu_{MA} peptide for which ion channel activity in planar lipid bilayers was demonstrated recently (*10*).

CD Spectroscopy. A CD analysis was performed to obtain initial information about the structure and folding of Vpu_{MA} and, more importantly, to define the optimal solution conditions for subsequent NMR experiments. In particular, our previous structural investigation of Vpu_{CYTO} indicated that Vpu, as with other membrane proteins, requires organic solvents to adopt stable secondary structure in solution. For this reason, the peptide Vpu^{1-39} was investigated in aqueous solution containing increasing amounts of TFE (Figure 1). The form of the curves with negative ellipticities at 208 and 220 nm and a positive band at ca. 190 nm is indicative of a significant amount of mainly α-helical structure that is present even at the lowest TFE content. Estimation of the helical content by standard methods (*42*) shows the presence

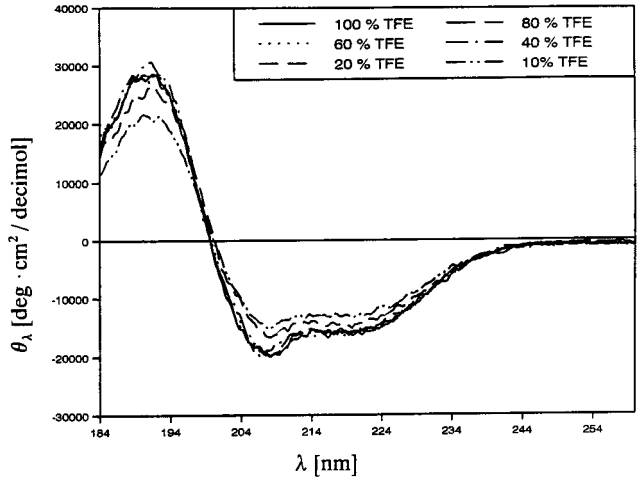

FIGURE 1: CD measurements of Vpu_a^{1-39} at various TFE concentrations.

of ca. 55% helix. Surprisingly, the CD curves show that the secondary structure is almost independent of the TFE content of the aqueous solvent. The fact that the extrema of the curves in 10 and 20% TFE are somewhat smaller but have the same distribution of minima and maxima as observed in all other cases probably arises from a concentration effect and not from a structural effect, especially as the peptide solubility was limited at lower TFE concentrations.

To guarantee maximal solubility even at low TFE concentrations, we analyzed a variant peptide, Vpu_a^{1-39}, that corresponds to the sequence of another biological active Vpu protein derived from the HIV-1 isolate NL4-3 (*2*, *4*, *32*). Although the Vpu_{MA} region is conserved among different HIV-1 isolates, a substantial polymorphism occurs within the first six N-terminal residues (*32*). Since the peptide Vpu_a^{1-39} appeared to have maximal solubility in aqueous TFE, this peptide was used for the CD analysis whose results are depicted in Figure 1.

The changes in the CD spectra of Vpu_a^{1-39} observed for different TFE concentrations in this study (Figure 1) are quite different from those previously found for fragments (*28*) or of the entire polar domain from Vpu_{CYTO} (*27*) where stable secondary structure was only present at TFE concentrations of >50%. This indicates that the α-helical region in Vpu_{MA}, in contrast to the helices in the cytoplasmic region of Vpu, adopts a stable α-helical conformation even at the lowest TFE concentrations. This observation may imply that the peptide would maintain its α-helical structure even without a strong membrane-like environment. Although the CD data indicated there is little change in the structure on going from 10 to 50% TFE, the solubility of the peptide was such that 50% TFE provided the best conditions for recording subsequent NMR spectra and thus allowed comparison with our previous work on Vpu_{CYTO} and its binding partner, the cytoplasmic tail of CD4 (*43*).

Secondary Structure in Solution from the α-Proton Chemical Shifts and Qualitative NOE Data. The chemical shift data from our experiments can be used to estimate the presence of secondary structure elements present in the molecule (*44*) as upfield shifts of the α-proton (Hα) in four adjacent residues relative to the random coil values are indicative of local helical structure. Alternatively, β-sheets are recognized as downfield shifts of three adjacent residues.

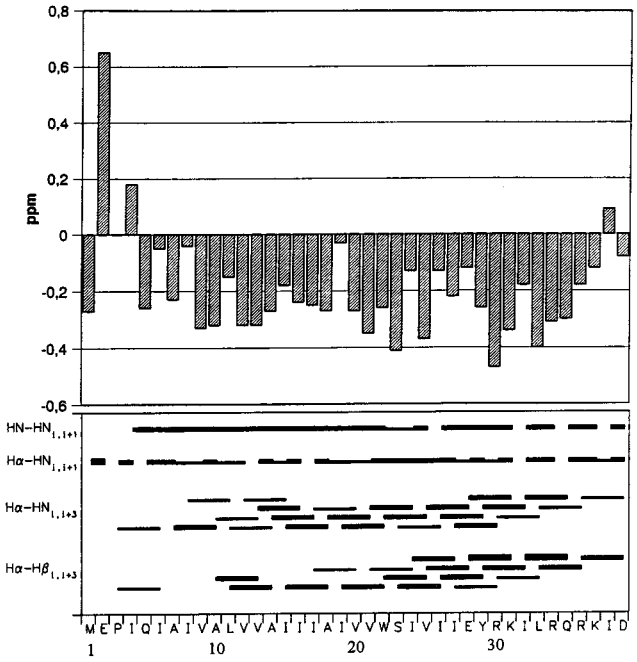

FIGURE 2: Chemical shift differences (parts per million) of the α-protons between the experimental values in 50% TFE and those for residues in a random coil for Vpu^{1-39} (upper panel) and a summary of the observed short- and medium-range NOEs for Vpu^{1-39} (lower panel). Five long-range NOEs were observed between Trp-22 (four) and Ile-26 (one) and Ala-7.

In the case of Vpu^{1-39}, the relative Hα shifts (Figure 2) are indicative of considerable helical content within a large region of the molecule bounded by residues Val-9−Lys-37 of the peptide. This is supported by the observation of a series of regular Hα−$HN_{i,i+3}$ and Hα−$H\beta_{i,i+3}$ NOEs in the same region (Figure 2). A single linear helix, however, extending from the region of residues 7−9 to the C-terminus of Vpu^{1-39} would not be consistent with the unambiguously identified long-range NOEs found between the side chains of Trp-22 and Ile-26 and Ala-7 (see the legend of Figure 2) that are indicative of a stable folded tertiary structure. The identity of these long-range NOEs was confirmed by comparing the structure of Vpu^{1-39}, the sequence of which was derived from the HIV-1 isolate HXB10 (*32*), with that of the fully assigned data obtained from studies on a variant peptide, Vpu_b^{1-39}. The sequence of the control peptide Vpu_b^{1-39} was derived from another HIV-1 isolate, LAI (*32*), and carries a single amino acid exchange (Glu-2 to Gln-2). The fact that both peptides had almost identical structures supports our hypothesis of structural conservation in Vpu_{MA} among different HIV-1 isolates, although considerable polymorphism is noticed within the first six N-terminal residues of Vpu_{MA} sequences derived from different virus isolates (*32*). It is, therefore, justifiable to assume that this conserved structure in Vpu_{MA} is critical for the ion channel function of Vpu, an activity that when analyzed in lipid bilayers or biological membranes was previously shown to depend on the integrity of Vpu_{MA} (*10*, *13*).

Noteworthy also are the considerable downfield shifts of Hα of Glu-2 and Ile-4 (Figure 2) that appear to point to a structured N-terminus which is quite unusual for a small peptide as such molecules usually have free, unstructured termini. A possible ring current effect from aromatic near neighbors can be discounted for these residues as there are

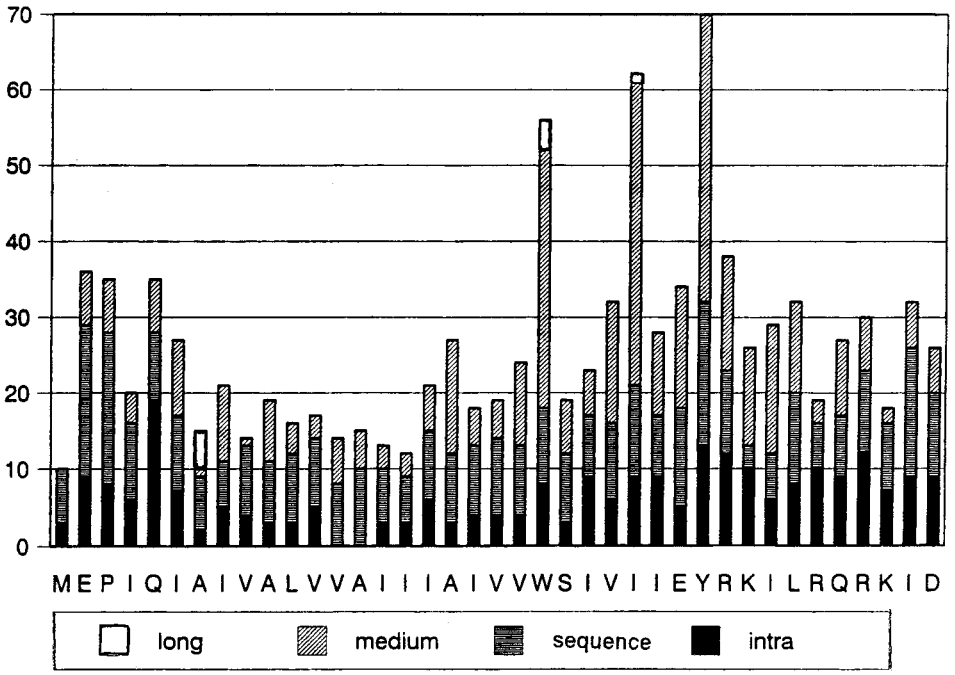

FIGURE 3: Distribution of the quantitative NOEs of Vpu^{1-39} used in the restrained MD structure calculations. Each NOE appears twice in this scheme as both residues, to which the interacting protons are attached, are shown. On average, 16 NOEs per residue were observed.

none in the near vicinity, although such an effect would account for the unusual high-field shift of the Hα of Ile-19 which is three residues away from Trp-22 and hence close to the aromatic system within the α-helical structure.

Final Solution Structure of Vpu^{1-39}. In a next step, the exact nature of the folded structure in Vpu^{1-39} was deduced from structural calculations using the quantitative NOE data. After quantitation of the NOE data, 642 NOEs (255 intra, 192 sequence, 190 medium-range, and 5 long-range), which are well-distributed over the entire sequence (Figure 3), were used as distance restraints to calculate structures that are compatible with the data. Of particular interest was how the five long-range NOEs would affect the MD calculations. A satisfactory solution was obtained only when no large violations in the bond lengths and angles occurred upon introduction of these NOEs into the calculation. Such a situation indicated that these important structural restraints were correctly assigned and a false structure had not been calculated. To be absolutely sure of the positions and hence assignments of the protons involved in these long-range interactions, we compared the NOESY spectra of the peptide Vpu^{1-39} with that of the variant peptide $Vpu_b{}^{1-39}$. In both cases, identical interactions were observed, supporting again our notion of a conserved structure among polymorphic Vpu_{MA} sequences derived from different HIV-1 isolates. No further long-range interactions were found in either peptide. In a final round of calculations involving all the NOEs measured for Vpu^{1-39}, 700 structures were calculated and 18 of these, in which the NOE energy was smaller than 58.6 kJ/mol and the sum of all the energy terms smaller than 347.3 kJ/mol, were chosen for the final analysis. The structure with the lowest energies had values of 44.8 and 307.9 kJ/mol, respectively, and all 18 final structures showed only very small deviations from these absolute lowest energies.

These calculations clearly show that the peptide Vpu^{1-39} has a well-defined tertiary structure (Figure 4). There is a turn at the N-terminus from Met-1 to Ile-6 that would account for the Hα downfield chemical shift changes noted above. This is followed by a linker (Ala-7−Val-9) that leads into a short helix from Ala-10 to Ile-16. A short loop region then leads into a second longer helix that stretches from Trp-22 to Arg-36 (Figure 4). This helix is not perfectly formed as it shows a bend at Tyr-29 (Figure 4C), which is well-defined through the many medium-range NOEs to neighboring residues. Thus, the peptide shows a relatively compact U-shaped structure formed by a loop that has the N-terminal linker and helix on one side and the second helix on the other side with the side chains of the two aromatic amino acids buried in the interior of the structure. The absence of any further long-range NOEs suggests there is little interaction between the domains in these structures, and hence, strong hydrophobic interactions are not present.

The areas of structural heterogeneity within the molecule may be assessed using the consecutive segment approach described by us previously (*41*) in which the rms differences for short segments two to five residues in length are systematically compared pairwise for all selected final structures. The average rms differences for all the backbone atoms are assigned to all residues in the segment chosen, and subsequently, the mean value is calculated for each residue after all segment lengths and all structures have been computed. These mean rms differences are then plotted against the residue number and afford a visual assessment of how well the backbone atom positions in each amino acid in all the final refined structures are defined on going from structure to structure. The result of this analysis for Vpu^{1-39} is shown in Figure 5. The mean rms differences found here are considerably smaller than those found in other linear peptides in the same solvent mixture that we have investigated previously (*41*, *43*) and confirm the rigidity of the calculated structure of Vpu^{1-39}. Comparison of Figure 5 with the distribution of quantitative NOE data used in the restrained MD calculations of Figure 3 indicates structural heterogeneity is not caused by the absence or limited amount

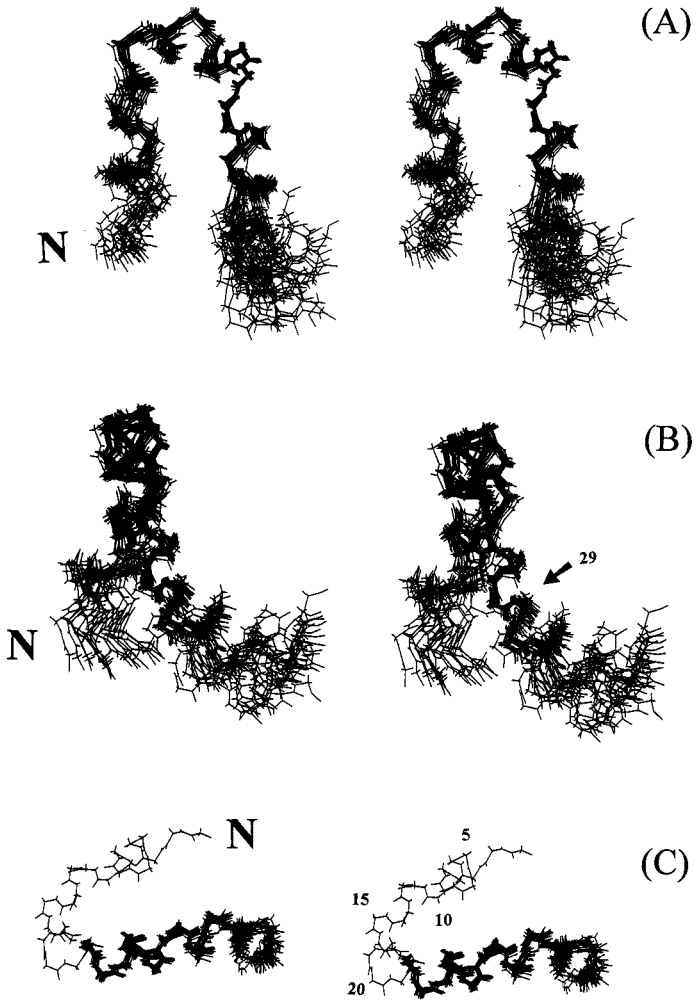

FIGURE 4: Stereoview superposition of the 18 best final restrained structures of Vpu^{1-39} in 50% TFE after alignment of backbone atoms Ile-6−Arg-30 (A and B) and Trp-22−Asp-39 (C). In panel A, the N-terminus is to the left and in panel B above the plane. Residue numbering has been included in panel C to facilitate the recognition of regions described in the text, and the discontinuity in the longer helix at residue 29 is indicated in panel B.

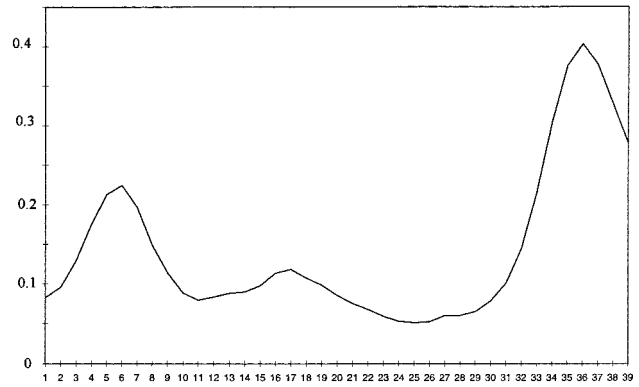

FIGURE 5: Mean rms differences for the backbone atoms in each residue, calculated using a consecutive segment method, plotted against the residue number. The regions of greatest heterogeneity are between and include residues 5−7 and 32−39, while the most stable region of the molecule is from residue 9 to 31 with somewhat more flexible residues in positions 16 and 17.

of NOE data. Consequently, the poorer definition of regions in the peptide appears to arise from increased flexibility and dynamics within the molecule. Consistent with the α-proton shifts (Figure 2), the end residues in the N-terminus again appear to be structured. Within the molecule, the most flexible regions are between residues 5 and 7 at the start of the short linker leading into the first α-helix and the fraying of the second helix starting at residue Ile-32 toward the C-terminus. The central most stable region of the molecule from residue Val-9 to Lys-31 shows poorer definition at the start of the loop (residues Ile-16−Ala-18) connecting the two helices within the U-shaped fold, although this interconnecting section is better defined than those regions near or at the peptide termini.

Structure of Vpu^{1-27} in Lipid Bilayers by Solid-State NMR. The compact U-folded solution structure of Vpu^{1-39} is such that it is unlikely to be able to cross a bilayer and is thus difficult to accommodate with the finding that the hydrophobic N-terminus of Vpu forms an ion-conductive membrane pore (*10*). To attempt to rationalize these findings, we have investigated the behavior of Vpu_{MA} in oriented phospholipid bilayers by solid-state NMR. This has the advantage of providing details about the orientation and topology of membrane-bound proteins and peptides in a lipid bilayer environment. For this study, synthetic peptides were used that were differentially labeled with ^{15}N and comprise the complete Vpu_{MA} region without any parts of the polar Vpu_{CYTO} domain. An unlabeled version of this peptide, Vpu^{1-27}, was previously used for electrophysiological studies in planar lipid bilayers (*10*). Figure 6 shows the proton-

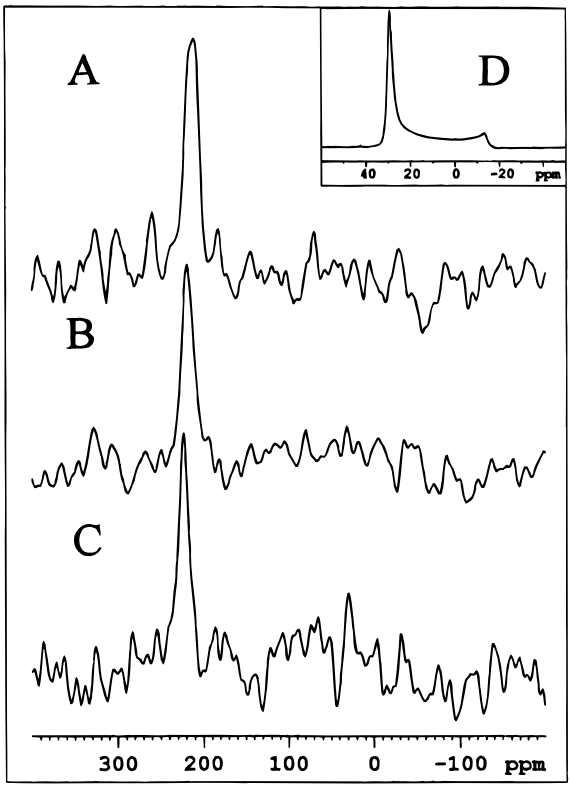

FIGURE 6: ^{1}H-decoupled ^{15}N spectra of 1.3 mol % ^{15}N-labeled Vpu$^{1-27}$ in oriented POPC lipid bilayers hydrated at 93% relative humidity. Vpu$^{1-27}$ with single backbone labels incorporated into alanine at positions 10 (A), 14 (B), and 18 (C) has chemical shifts of 210, 218, and 220 ppm, respectively. Inset D shows a representative ^{31}P spectra of the same sample used to measure the spectrum shown in panel A.

decoupled ^{15}N cross polarization solid-state NMR spectra of three Vpu$^{1-27}$ peptides differentially labeled with ^{15}N in positions Ala-10, Ala-14, and Ala-18, and oriented in phospholipid bilayers. The peptide samples have been well aligned with the membrane normal parallel to the magnetic field direction; hence, the orientationally dependent solid-state NMR parameters can be related directly to the molecular orientation of the peptide within the lipid bilayer (*31*, *46*−*48*). Measurement of several solid-state NMR parameters per peptide bond provides sufficient structural constraints to determine the backbone structure of membrane-associated polypeptides (*49*, *50*). Whereas the spectral width of an unoriented polypeptide sample labeled at a single alanine site would exhibit a broad powder pattern line shape between 58 and 234 ppm (*31*, *51*−*53*, *58*, *71*), the ^{15}N spectra recorded here exhibit line widths at half-height of <20 ppm, indicating that the peptides are well-oriented with respect to the magnetic field direction. All three labeled sites resonate at chemical shifts of >200 ppm, indicating a transmembrane alignment of helical polypeptides (*31*, *48*, *54*). Figure 6D shows a ^{31}P NMR spectrum that is representative of all three samples and serves as an indicator of the orientational distribution of the phospholipid headgroups with respect to the bilayer normal. The lipids predominantly resonate at a ^{31}P chemical shift of 30 ppm typical of phosphatidylcholine molecules in liquid crystalline lipid bilayers that are oriented with their normal parallel to the magnetic field direction. Small contributions between 30 and -15 ppm are also observed and can be attributed to differently aligned liquid crystalline lipids and/or conformational changes of the phospholipid headgroup due to the presence of the Vpu$^{1-27}$ peptide (*45*). The ^{31}P NMR spectra of Vpu$^{1-27}$ in POPC lipid bilayers exhibit line shapes similar to those reported recently for influenza A virus M2 peptides in hydrated dimyristoylphosphatidylcholine bilayers (*55*). In contrast, the proton-decoupled ^{15}N resonances were more dispersed than those found here.

To test for possible conformational changes during the reconstitution of Vpu$_{MA}$ from organic solvents into hydrated lipid bilayers, the structure of the Vpu$^{1-39}$ core region obtained in TFE solution was compared with the experimental solid-state NMR ^{15}N chemical shifts measured in oriented lipid bilayers. In the first step of these calculations, the static ^{15}N chemical shift tensor was oriented with respect to the molecular coordinate system of the polypeptide structure using a Euler algorithm. The chemical shift tensor describes the orientationally dependent interactions of the ^{15}N nuclei with the magnetic field of the NMR spectrometer. Static ^{15}N chemical shift tensors have been characterized previously using a variety of ^{15}N-labeled model peptides (*51*, *52*, *56*). The tensor of the amide bond exhibits only a moderate functional dependence with respect to the secondary structure of the polypeptide chain or the chemical nature of the amino acid side chains (although larger deviations are observed with glycine) (*57*, *58*).

In the next step, a Cartesian coordinate system was defined in the laboratory frame in which the *z*-axis coincided with the magnetic field direction of the NMR spectrometer and the perpendicular axes were chosen arbitrarily. The molecule was rotated around the *x*- and *y*-axes in the laboratory frame to obtain all possible orientations of the polypeptide with respect to the magnetic field direction. For every molecular orientation, the resulting ^{15}N chemical shift values of the three labeled sites are calculated and visualized as a contour plot. Rotation of the molecule around the *x*- and *y*-axes of the laboratory frame is shown in Figure 7 in which lines depict the angular pairs for the three labeled sites in Vpu$^{1-27}$ that are in agreement with the three measured ^{15}N chemical shift values of 210 (Ala-10), 218 (Ala-14), and 220 ppm (Ala-18). When the conformation of the Vpu$^{1-39}$ molecule obtained by solution NMR in TFE was used as the model, it is evident that there is no single molecular orientation that would explain all three ^{15}N chemical shifts of the peptide in uniaxially oriented lipid bilayers (Figure 7A). Major structural rearrangements of the polypeptide backbone involving the loss of the folded tertiary structure during the insertion into a lipid bilayer are required for the three contours of the measured solid-state ^{15}N chemical shift to meet in at least one point. The uncertainty in determining the chemical shift value is less than ± 5 ppm and when taken into consideration results in an increased number of angular pairs that agree with the experimental solid-state NMR data. This can be visualized by widening the contour lines and is illustrated with residue Ala-10 in Figure 7A. Furthermore, the static chemical shift tensors which were used in these calculations have been determined experimentally and exhibit uncertainties in their principal values as well as in their alignment within the molecular coordinate system (*31*, *51*−*53*, *56*−*58*, *71*). These uncertainties have been considered during different sets of calculations in which a wide range of published main tensor elements has been applied to the

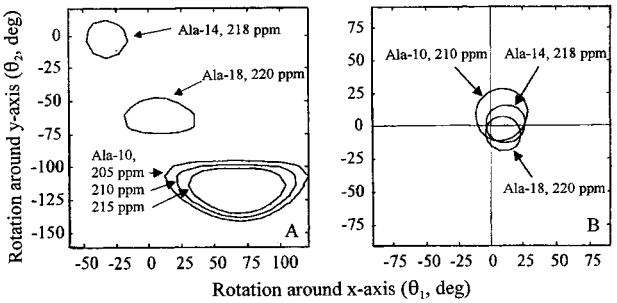

FIGURE 7: Contour plot of the ^{15}N chemical shift tensor calculated on the basis of the lowest-energy final conformation found for the solution structure of Vpu$^{1-39}$ in 50% TFE (A) and an ideal α-helix (B). The two graphical axes correspond to rotation of the molecules around two axes perpendicular to the magnetic field. For a given structure to agree with the experimental ^{15}N solid-state NMR data of all labeled sites, the contours have to meet in at least one point. (A) According to this criterion, the solution structure of the segment of residues 10−18 of the Vpu$^{1-39}$ structure obtained in TFE is inconsistent with the solid-state NMR data recorded for Vpu$^{1-27}$ in oriented lipid bilayers. (B) An ideal linear α-helix with a tilt angle of ≤30° with respect to the bilayer normal would perfectly fit the measured data. The principal axis values (68, 93, and 227 ppm) and their alignment within the molecular coordinate system used for these calculations were taken from those published for alanine in a hydrated peptide (*71*). Additional contours shown for Ala-10 exemplify the increase in possible molecular orientations due to an error of ±5 ppm during the chemical shift determination (see the text for details).

experimental data. The variance in these tensor elements results in a further increase in the number of possible molecular orientations that are in agreement with a measured chemical shift value. This tensor-related uncertainty increases the number of potential orientations that would agree with a measured chemical shift by an additional extent comparable to the one that has already been indicated by the error bars for the oriented chemical shift determination shown in Figure 7A.

In a second round of calculations presented in Figure 7B, a linear α-helical model structure for the peptide was assumed with the initial orientation of the helix parallel to the *z*-axis. The three contours now approach each other and show some overlap which implies the model is compatible with the measured solid-state NMR data. The experimental chemical shift values indicate that the best correspondence for an ideal α-helix occurs when the helix is tilted by ≤30° with respect to the bilayer normal (*z*-axis). The tilt angle γ can be deduced from Figure 7A as it is a function of θ_1 and θ_2. If motional averaging reduces the apparent chemical shift tensor element σ_{33} by <8 ppm, the helix tilt angle remains within the limits given above (not shown).

In summary, the experimental solid-state ^{15}N NMR data for Vpu$^{1-27}$ are incompatible with the molecule adopting the same folded structure as that found in TFE solution and are in agreement with a linear α-helix that lies parallel to the bilayer normal with a tilt angle of ≤30°.

DISCUSSION

Here, for the first time, we have experimentally established details of the secondary structure and membrane orientation of the ion channel forming Vpu$_{MA}$ domain. The high-resolution structure and tertiary fold of Vpu$_{MA}$ and its connection to the adjacent polar domain Vpu$_{CYTO}$ were elucidated using a combination of CD and ^{1}H NMR spectroscopy in aqueous TFE. Subsequently, the position of Vpu$_{MA}$ in a membrane has been studied in oriented lipid bilayers by solid-state ^{15}N NMR techniques. Results from both solid-state and solution NMR techniques agree on the existence of a predominantly α-helical structure for Vpu$_{MA}$. Clearly, however, there is a major structural difference detected by studies of the bilayer-bound peptide and that in aqueous TFE. The discrepancy lies in the linearity of the helical region; while solid-state NMR provides evidence for a single linear helix that penetrates the lipid bilayer in a transmembrane fashion, the same region in solution adopts a U-shaped tertiary fold incorporating a number of short helices and linker regions.

The NMR data presented here afford convincing evidence for the presence of a well-defined tertiary structure for the peptide Vpu$^{1-39}$ even in 50% aqueous TFE in addition to helical secondary structure. The U-shaped compact structure is comprised of an N-terminal turn (residues 1−6), a linker (residues 7−9), and a short helix (residues 10−16) followed by a loop to a second longer helix (residues 22−36) incorporating a bend at residue 29. In this structure, the two aromatic residues (Trp-22 and Tyr-29) are directed toward the center of the molecule around which the hydrophobic core is positioned. The distance between the centers of the two aromatic systems (>4.5 Å) is too large to invoke a stacking interaction, but the aromatic rings presumably allow favorable weak hydrophobic interactions with adjacent helical sections of the molecule, although these do not lead to detectable NOE interactions. In this compact structure, the side chains of the two negatively charged residues (Glu-2 and Glu-28), the hydrophilic residues (Gln-5 and Ser-23), and the positively charged residues (Arg-30 and Lys-31) have relatively well-defined conformations and point out away from the central hydrophobic core and into the polar medium. The poorer definition and hence increased flexibility of the C-terminal residues (Ile-32−Asp-39) observed in Figure 5 probably arise from favorable intermolecular interactions with solvent of the considerable number of charged residues rather than from the lack of structure-stabilizing intramolecular interactions.

The presence of a defined tertiary structure in aqueous organic solutions is in distinct contrast to most previous studies of peptides incorporating membrane-spanning regions of larger proteins (*59*, *60*) where predominantly α-helical structures were found without any evidence of well-defined tertiary structure. An exception is the C-subunit of F_1F_0-ATPase which folds as a hairpin of two antiparallel helical segments (*61*, *62*). However, inspection of the primary sequences of those peptides without tertiary structures shows that within each of the membrane anchor domains there are a number of polar and/or charged residues that presumably undergo favorable interactions with the solvent that would destabilize any tendency to form tertiary structure. In contrast, the sequence of Vpu$_{MA}$ is unusual inasmuch as its center is totally hydrophobic in nature and is largely comprised of residues with branched aliphatic side chains (of the 16 hydrophobic residues between positions 6 and 21, 12 are branched followed by another 4 branched residues before Glu-28, the first charged residue in Vpu$_{CYTO}$). The peculiarity of Vpu$_{MA}$ becomes particularly obvious on comparison with the transmembrane domain of the influenza A virus M2 protein (M2$_{TM}$). Like Vpu, M2 is a multifunctional single-

span oligomeric ion channel-forming (*63*) class I integral membrane phosphoprotein with a membrane anchor and a polar cytoplasmic domain comparable to the size of that of Vpu (*64*). Sequence alignment of both, Vpu_{MA} and $M2_{TM}$, indicates only four nonconserved amino acid exchanges located exactly in the region known to be important for interaction of $M2_{TM}$ with the ion channel blocker amantadine (Val-27, Ser-31, and Gly-34 in $M2_{TM}$) and known to be important for the gating of the M2 channel activity by pH (His-37 in $M2_{TM}$) (*63*, *65*, *66*). In contrast to M2, the Vpu ion channel activity is not sensitive to amantadine and is not activated by pH (*10*). Thus, while polar residues are centered in the middle of $M2_{TM}$ (Ser-31 and His-37) they are shifted toward the C-terminal end in Vpu_{MA} (Trp-22 and Ser-23). This may explain the unusual tertiary fold observed for Vpu^{1-39} in solution and the differences in the electrophysiology of both channel proteins (*10*, *11*, *63*).

Careful inspection of Figure 4 indicates that the linker and loop regions have the same backbone turn direction as those of the well-defined helices and suggests that the structure has undergone distortion away from a linearly extended α-helix incorporating at least residues 9−31 to accommodate the intramolecular hydrophobic interactions that favor the compact structure. This folded structure observed in aqueous TFE for Vpu^{1-39} is clearly not maintained when Vpu_{MA} was analyzed by solid-state NMR in the strong hydrophobic environment of the bilayer. Our data point to the peptide being immobilized by its interactions with the membrane; otherwise, no ^{15}N spectrum would be obtained by cross polarization, or the signals would be very close to the isotropic value. In contrast, the chemical shifts for all three ^{15}N-labeled peptides are close to the downfield edge of the static chemical shift anisotropy (>200 ppm) and, therefore, are indicative of a helical domain oriented approximately parallel to the bilayer normal. If it is assumed that the U-formed structure established in solution also exists in membranes, then the individually ^{15}N-labeled alanine residues in positions 10, 14, and 18 of Vpu_{MA} should have different orientations with respect to the bilayer surface, irrespective of the orientation of the total structure in the bilayer. The ^{15}N chemical shifts, however, are indicative of only one single helical conformation in Vpu_{MA} involving residues 10−18. This helix is almost orthogonal to the bilayer surface without any evidence of a dynamic conformational equilibrium, including a folded structure such as the one shown in Figure 4. The simplest rationale would be that the molecule has adopted a single linear or near-linear transmembrane helix.

This general structure established for Vpu_{MA} is similar to that recently found experimentally by Kovacs and Cross for the influenza A virus $M2_{TM}$ under membrane conditions using a very similar solid-state NMR approach. As with Vpu, the ^{15}N chemical shift data of $M2_{TM}$ indicate the molecule assumes a uniform trans-oriented α-helix in lipid bilayers with a tilt angle of approximately 33° (*55*). Hence, the monomer has the same orientation as and a tilt angle similar to that of the ones found here for Vpu_{MA}. On the basis of previously reported biochemical data for disulfide bond formation and oligomerization of M2 (*64*, *68*), the authors further argued that this motif exists as a left-handed four-helix bundle (*55*). Currently, this model differs from that of Vpu_{MA} where a pentameric bundle without the possibility of disulfide bond formation has been suggested from modeling (*24*, *25*). In addition, modeling studies with a Vpu_{MA} sequence that excluded the first five polar N-terminal residues suggest the existence of a conical helix bundle that would be unable to support a continuous water column necessary for forming an ion channel in the opened state (*25*). Indeed, the ion channel function of Vpu (*10*, *11*, *13*) was recently challenged by the findings of Coady et al. (*67*), suggesting that Vpu expressed in amphibian oocytes exerts its effect on membrane currents most likely by modulating the stability of host cell membrane proteins rather than through direct ion channel formation. Hence, further studies on the molecular structure and function of full-length Vpu in artificial and natural membranes are necessary to clarify the mechanisms by which Vpu's unusual Vpu_{MA} domain affects membrane conductance and thereby augments virus particle release from the cell membrane of HIV-1-infected cells (*13*).

It should also be noted that the solid-state data presented here indicate the peptide is immobilized by its interactions with the lipid bilayer. Additional information about the dynamics are difficult to deduce from these data, and therefore, little can be concluded concerning the oligomerization of Vpu_{MA} in membranes. Oligomerization would reduce the extent of diffusion around the transmembrane helix axis (that is the bilayer normal/magnetic field direction) and, therefore, hardly influence the spectra. In the current state, our experiments do not afford the conformation of the peptide in the pore structure, although the conformation and topology of the monomer might be close to its structure in the oligomeric state.

The question now arises as to the length and extent of the transmembrane helix. The solution data suggest that the helix does not begin before residue 5 or 6 in the N-terminus but is present by or before residue 10. This is supported by the solid-state NMR data that require an immobilized conformation to be present in which the NH vectors exhibit a similar well-defined orientation between at least residues 10−18. This requires the loss in the membrane of the loop region found in solution between residues 17 and 21. Thus, the helix could now extend in the membrane to at least residue 29 and include the well-defined helical region between Trp-22 and Tyr-29 found in solution. A disruption and change in orientation at this latter residue are supported by the bend in the helix observed for the C-terminus of Vpu_{MA} in the solution structure. Thus, although our data from solution and solid-state NMR are not unequivocal, they are compatible with a transmembrane helix approximately 20−23 residues in length that, in the case of full-length Vpu, places the aromatic residues near to (Trp-22) and at (Tyr-29) the membrane−cytoplasm interface. It also places the hydrophilic and charged residues in this region at the periphery or outside the membrane. As a peptide sequence of 17−20 amino acids is required to span the lipid bilayer in an α-helical conformation, the tilt angle deduced from our oriented solid-state NMR experiments is in good agreement with the above considerations and ensures that the maximum number of hydrophobic residues are in contact with the lipid bilayer core.

Thus, the model of the N-terminal domain described here can now be correlated with that of the cytoplasmic domain of full-length Vpu in which the first helical region was found

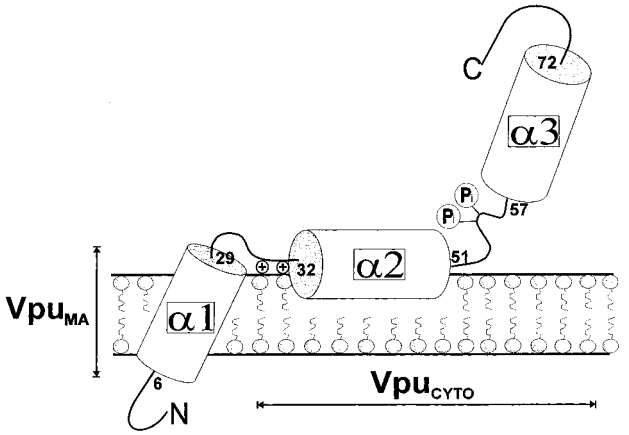

FIGURE 8: Model of the membrane-associated structure of monomeric full-length Vpu. Amino acid positions of helices α1−α3 are indicated; P_i represents phosphoseryl residues in positions 52 and 56.

between residues 37 and 51 (*27*, *28*). The increased flexibility apparent in the solution structure for residues 32−37 that are predominantly positively charged would afford a linker region between the strictly hydrophobic Vpu_{MA} helix (α1 in Figure 8) and an initial amphipathic helix in Vpu_{CYTO} (α2 in Figure 8). It is conceivable that the first cytoplasmic helix α2 could extend N-terminally as its amphipathic character could be maintained to residue 32 on the basis of our previous NMR studies with peptides of Vpu_{CYTO} (*27*, *28*). Our present experimental observations indicate that α1 spans the bilayer with its main axis perpendicular to the membrane surface while α2 probably swims in the interfacial region of the bilayer with its axis parallel to the membrane surface as this is characteristic of such amphipathic helices (*69*) and is commonly encountered in membrane-binding peptide antibiotics (*49*, *70*). The position of the third helix, α3, and C-terminal loop with respect to the cytosolic face of the ER membrane is more difficult to predict and must await further studies. However, this arrangement (Figure 8) of anchor helix α1 and the previously characterized cytoplasmic helix α2 would allow independent mobility of these helices that would not hinder oligomerization of Vpu_{MA} in forming ion-conductive membrane pores (*24*, *25*). Clearly, future solid-state NMR studies with sequences comprising both domains, Vpu_{MA} and Vpu_{CYTO}, will provide more insight into the topology of full-length Vpu in membranes.

ACKNOWLEDGMENT

We are indebted to J. W. Yewdell and J. R. Bennink for their support and to M. Helmle and B. Vogt for their valuable help with the tensor calculations.

SUPPORTING INFORMATION AVAILABLE

Table of ^{1}H NMR assignments and chemical shifts (in parts per million) of Vpu^{1-39} in 50 vol % TFE at 299 K and pH 3.7. This material is available free of charge via the Internet at http://pubs.acs.org.

REFERENCES

1. Cohen, E. A., Terwilliger, E. F., Sodroski, J. G., and Haseltine, W. A. (1988) *Nature 334*, 532−534.
2. Strebel, K., Klimkait, T., and Martin, M. A. (1988) *Science 241*, 1221−1223.
3. Huet, T., Cheynier, R., Meyerhans, A., Roelants, G., and Wain-Hobson, S. (1990) *Nature 345*, 356−358.
4. Strebel, K., Klimkait, T., Maldarelli, F., and Martin, M. A. (1989) *J. Virol. 63*, 3784−3791.
5. Klimkait, T., Strebel, K., Hoggan, M. D., Martin, M. A., and Orenstein, J. M. (1990) *J. Virol. 64*, 621−629.
6. Maldarelli, F., Chen, M.-Y., Willey, R. L., and Strebel, K. (1993) *J. Virol. 67*, 5056−5061.
7. Chen, M.-Y., Maldarelli, F., Karczewski, M. K., Willey, R. L., and Strebel, K. (1993) *J. Virol. 67*, 3877−3884.
8. Schubert, U., Schneider, T., Henklein, P., Hoffmann, K., Berthold, E., Hauser, H., Pauli, G., and Porstmann, T. (1992) *Eur. J. Biochem. 204*, 875−883.
9. Schubert, U., Henklein, P., Boldyreff, B., Wingender, E., Strebel, K., and Porstmann, T. (1994) *J. Mol. Biol. 236*, 16−25.
10. Schubert, U., Ferrer-Montiel, A. F., Oblatt-Montal, M., Henklein, P., Strebel, K., and Montal, M. (1996) *FEBS Lett. 398*, 12−18.
11. Ewart, G. D., Sutherland, T., Gage, P. W., and Cox, G. B. (1996) *J. Virol. 70*, 7108−7115.
12. Terwilliger, E. F., Cohen, E. A., Lu, Y., Sodroski, J. G., and Haseltine, W. A. (1989) *Proc. Natl. Acad. Sci. U.S.A. 86*, 5163−5167.
13. Schubert, U., Bour, S., Ferrer-Montiel, A. F., Montal, M., Maldarelli, F., and Strebel, K. (1996) *J. Virol. 70*, 809−819.
14. Willey, R. L., Maldarelli, F., Martin, M. A., and Strebel, K. (1992) *J. Virol. 66*, 226−234.
15. Kerkau, T., Bacik, I., Bennink, J. R., Yewdell, J. W., Hünig, T., Schimpl, A., and Schubert, U. (1997) *J. Exp. Med. 185*, 1295−1305.
16. Bour, S., Schubert, U., and Strebel, K. (1995) *J. Virol. 69*, 1510−1520.
17. Schubert, U., and Strebel, K. (1994) *J. Virol. 68*, 2260−2271.
18. Paul, M., and Jabbar, M. A. (1997) *Virology 232*, 207−216.
19. Friborg, J., Ladha, A., Goettlinger, H., Haseltine, W. A., and Cohen, E. A. (1995) *J. Acquired Immune Defic. Syndr. Hum. Retrovirol. 8*, 10−22.
20. Margottin, F., Bour, S. P., Durand, H., Selig, L., Benichou, S., Richard, V., Thomas, D., Strebel, K., and Benarous, R. (1998) *Mol. Cell 1*, 565−574.
21. Fujita, K., Omura, S., and Silver, J. (1997) *J. Gen. Virol. 78*, 619−625.
22. Schubert, U., Anton, L. C., Bacik, I., Cox, J. H., Bour, S., Bennink, J. R., Orlowski, M., Strebel, K., and Yewdell, J. W. (1998) *J. Virol. 72*, 2280−2288.
23. Lamb, R. A., and Pinto, L. H. (1997) *Virology 229*, 1−11.
24. Grice, A. L., Kerr, I. D., and Sansom, M. S. P. (1997) *FEBS Lett. 405*, 299−304.
25. Moore, P. B., Zhong, Q., Husslein, T., and Klein, M. L. (1998) *FEBS Lett. 431*, 143−148.
26. Henklein, P., Schubert, U., Kunert, O., Klabunde, S., Wray, V., Klöppel, K.-D., Kiess, M., Porstmann, T., and Schomburg, D. (1993) *Pept. Res. 6*, 79−87.
27. Federau, T., Schubert, U., Flossdorf, J., Henklein, P., Schomburg, D., and Wray, V. (1996) *Int. J. Pept. Protein Res. 47*, 297−310.
28. Wray, V., Federau, T., Henklein, P., Klabunde, S., Kunert, O., Schomburg, D., and Schubert, U. (1995) *Int. J. Pept. Protein Res. 45*, 35−43.
29. Willbold, D., Hoffmann, S., and Rösch, P. (1997) *Eur. J. Biochem. 245*, 581−588.
30. Cross, T. A., and Opella, S. J. (1994) *Curr. Opin. Struct. Biol. 4*, 574−581.
31. Bechinger, B., Kim, Y., Chirlian, L. E., Gesell, J., Neumann, J.-M., Montal, M., Tomich, J., Zasloff, M., and Opella, S. J. (1991) *J. Biomol. NMR 1*, 167−173.
32. Myers, G., Foley, B., Mellors, J. W., Korber, B., Jeang, K. T., and Wain-Hobson, S. (1996) *Human retroviruses and AIDS*, Los Alamos National Laboratory, Los Alamos, NM.
33. Adachi, A., Gendelman, H. E., Koenig, S., Folks, T., Willey, R. L., Rabson, A., and Martin, M. A. (1986) *J. Virol. 59*, 284−291.

34. Bechinger, B., and Opella, S. J. (1991) *J. Magn. Reson. 95*, 585−588.
35. Pines, A., Gibby, M. G., and Waugh, J. S. (1973) *J. Chem. Phys. 59*, 569−590.
36. Wüthrich, K. (1986) *NMR of Proteins and Nucleic Acids*, Wiley-Interscience, New York.
37. Niedig, K. P., and Kalbitzer, H. R. (1990) *J. Magn. Reson. 88*, 155−160.
38. Gronwald, W., Schomburg, D., Harder, M. P. F., Mayer, H., Paulsen, J., Wingender, E., and Wray, V. (1996) *Biol. Chem. Hoppe-Seyler 377*, 175−186.
39. Brünger, A. T. (1992) *X-PLOR, Version 3.1, A System for X-ray Crystallography and NMR*, Yale University Press, New Haven, CT.
40. Schomburg, D., and Reichelt, J. (1988) *J. Mol. Graphics 6*, 161−165.
41. Blankenfeldt, W., Nokihara, K., Naruse, S., Lessel, U., Schomburg, D., and Wray, V. (1996) *Biochemistry 35*, 5955−5962.
42. Greenfield, N., and Fasman, G. D. (1969) *Biochemistry 8*, 4108−4116.
43. Wray, V., Mertins, D., Kiess, M., Henklein, P., Trowitzsch-Kienast, W., and Schubert, U. (1998) *Biochemistry 37*, 8527−8538.
44. Wishart, D. S., Sykes, B. D., and Richards, F. M. (1992) *Biochemistry 31*, 1647−1651.
45. Scherer, P. G., and Seelig, G. (1989) *Biochemistry 28*, 7720−7727.
46. Smith, R., Separovic, F., Milne, T. J., Whittaker, A., Bennett, F. M., Cornell, B. A., and Makriyannis, A. (1994) *J. Mol. Biol. 241*, 456−466.
47. North, C. L., Barranger-Mathys, M., and Cafiso, D. S. (1995) *Biophys. J. 69*, 2392−2397.
48. Bechinger, B. (1996) *J. Mol. Biol. 263*, 768−775.
49. Bechinger, B., Zasloff, M., and Opella, S. J. (1993) *Protein Sci. 2*, 2077−2084.
50. Ketchem, R. K., Hu, W., and Cross, T. A. (1993) *Science 261*, 1457−1460.
51. Oas, T. G., Hartzell, C. J., Dahlquist, F. W., and Drobny, G. P. (1987) *J. Am. Chem. Soc. 109*, 5962−5966.
52. Hartzell, C. J., Whitfield, M., Oas, T. G., and Drobny, G. P. (1987) *J. Am. Chem. Soc. 109*, 5966−5969.
53. Wu, C. H., Ramamoorthy, A., Gierasch, L. M., and Opella, S. J. (1995) *J. Am. Chem. Soc. 117*, 6148−6149.
54. Bechinger, B., Gierasch, L. M., Montal, M., Zasloff, M., and Opella, S. J. (1996) *Solid State Nucl. Magn. Reson. 7*, 185−192.
55. Kovacs, F. A., and Cross, T. A. (1997) *Biophys. J. 73*, 2511−2517.
56. Teng, Q., and Cross, T. A. (1989) *J. Magn. Reson. 85*, 439−447.
57. Shoji, A., Ozaki, T., Fujito, T., Deguchi, K., Ando, S., and Ando, I. (1989) *Macromolecules 22*, 2860−2863.
58. Shoji, A., Ozaki, T., Fujito, T., Deguchi, K., Ando, S., and Ando, I. (1990) *J. Am. Chem. Soc. 112*, 4693−4697.
59. Doak, D. G., Mulvey, D., Kawaguchi, K., Villalain, J., and Campbell, I. D. (1996) *J. Mol. Biol. 258*, 672−687.
60. Gargaro, A. R., Bloomberg, G. B., Dempsey, C. E., Murray, M., and Tanner, M. J. A. (1994) *Eur. J. Biochem. 221*, 445−454.
61. Norwood, T. J., Crawford, D. A., Steventon, M. E., Driscoll, P. C., and Campbell, I. D. (1992) *Biochemistry 31*, 6285−6290.
62. Girvin, M. E., Rastogi, V. K., Abildgaard, F., Markley, J. L., and Fillingame, R. H. (1998) *Biochemistry 37*, 8817−8824.
63. Pinto, L. H., Holsinger, J., and Lamb, R. A. (1992) *Cell 69*, 517−528.
64. Sugrue, R. J., and Hay, A. J. (1991) *Virology 180*, 617−624.
65. Wang, C., Takeuchi, K., Pinto, L. H., and Lamb, R. A. (1993) *J. Virol. 67*, 5585−5594.
66. Wang, S., Lamb, R. A., and Pinto, L. H. (1995) *Biophys. J. 69*, 1363−1371.
67. Coady, M. J., Daniel, N. G., Tiganos, E., Allain, B., Friborg, J., Lapointe, J.-Y., and Cohen, E. A. (1998) *Virology 244*, 39−49.
68. Holsinger, L. J., and Lamb, R. A. (1991) *Virology 183*, 32−43.
69. Gilbert, G. E., and Baleja, J. D. (1995) *Biochemistry 34*, 3022−3031.
70. Kaiser, E. T., and Kezdy, F. J. (1987) *Annu. Rev. Biophys. Biophys. Chem. 16*, 561−581.
71. Lazo, N. D., Hu, W., and Cross, T. A. (1995) *J. Magn. Reson. 107*, 43−50.

BI982755C